Biochemistry

pubs.acs.org/biochemistry Article

NRVS and DFT of MitoNEET: Understanding the Special Vibrational Structure of a [2Fe-2S] Cluster with $(Cys)_3(His)_1$ Ligation

Leland B. Gee, Vladimir Pelmenschikov, Cécile Mons, Nakul Mishra, Hongxin Wang, Yoshitaka Yoda, Kenji Tamasaku, Marie-Pierre Golinelli-Cohen, and Stephen P. Cramer*

Cite This: *Biochemistry* 2021, 60, 2419–2424 Read Online

ACCESS | Metrics & More | Article Recommendations | Supporting Information

ABSTRACT: The human mitochondrial protein, mitoNEET (mNT), belongs to the family of small [2Fe-2S] NEET proteins that bind their iron–sulfur clusters with a novel and characteristic 3Cys:1His coordination motif. mNT has been implicated in the regulation of lipid and glucose metabolisms, iron/reactive oxygen species homeostasis, cancer, and possibly Parkinson's disease. The geometric structure of mNT as a function of redox state and pH is critical for its function. In this study, we combine ^{57}Fe nuclear resonance vibrational spectroscopy with density functional theory calculations to understand the novel properties of this important protein.

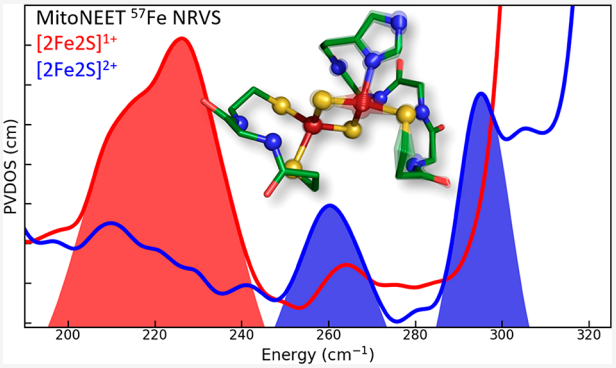

The NEET proteins comprise a family of small proteins that bind their iron–sulfur [2Fe-2S] clusters with a novel and characteristic 3Cys:1His coordination motif.[1] The human mitochondrial outer-membrane version, mitoNEET (mNT), was discovered as a potential target of insulin-sensitizing thiazolidinedione drugs.[2] It has since been found to be involved in the regulation of lipid and glucose metabolisms,[3,4] iron/reactive oxygen species homeostasis[4−6] with implication in cancer,[7−9] and possibly Parkinson's disease.[10] *In vitro* studies revealed that mNT can transfer its cluster to a recipient apoprotein[11] under the strict control of the redox state (only the oxidized cluster can be transferred)[12] and regulation by pH.[12] Using complementary *in cellulo* experiments, we demonstrated that mNT is involved in the pathway dedicated to reactivation of cytosolic aconitase after an oxidative/nitrosative stress. *In vitro*, mNT can transfer its clusters to the apo form of the cytosolic aconitase, or iron-regulatory protein (IRP-1), and reactivate it.[5] However, *in cellulo* it is unclear if the IRP-1 cluster is either fully destroyed or in the [3Fe-4S] form. Likewise, it is unknown if mNT could rebuild an active cluster in the [3Fe-4S] form of IRP-1.

Crystal structures[13−15] of mNT reveal a homodimeric fold with one [2Fe-2S] cluster per monomer and two domains: the β cap and a cluster binding domain, with the cluster domain shown in Figure 1.[13] The presence of a histidine ligand to one Fe site confers some unusual properties upon this cluster, including a pH-dependent redox potential higher than that of conventional [2Fe-2S] ferredoxin (Fd) proteins,[16] proton-coupled electron transfer (PCET) capability,[17,18] and redox control[19] and pH modulation[12] of its cluster transfer activity.

The mNT protein has already been studied by a variety of spectroscopies, including ultraviolet–visible,[5,20] electron paramagnetic resonance (EPR),[20−22] nuclear magnetic resonance (NMR),[5,19] Mössbauer,[5,20] and Raman[12,23] techniques, as well as molecular dynamics.[24,25] However, questions about the drastic difference in behavior concerning cluster stability and transfer between the reduced and oxidized forms of the protein remain. Especially important is the characterization of the Fe–His interaction through the coordinating N_δ atom. It has been proposed that this bond may play a role in cluster lability.[21,23]

To better understand the special properties of the mNT [2Fe-2S] cluster and to gain insights into the role of the coordinating histidine in cluster labilization, we have utilized ^{57}Fe nuclear resonance vibrational spectroscopy (NRVS) combined with density functional theory (DFT) calculations.

RESULTS AND DISCUSSION

NRVS at pH 6.7. In our previous studies,[12] we demonstrated that the stability of the oxidized form of mNT decreases at a more acidic pH. From pH 7.2 to 8, the oxidized form is quite stable; however, the cluster stability significantly decreases below pH 7. We decided to explore the oxidized and

Received: April 14, 2021
Revised: July 6, 2021
Published: July 26, 2021

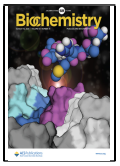

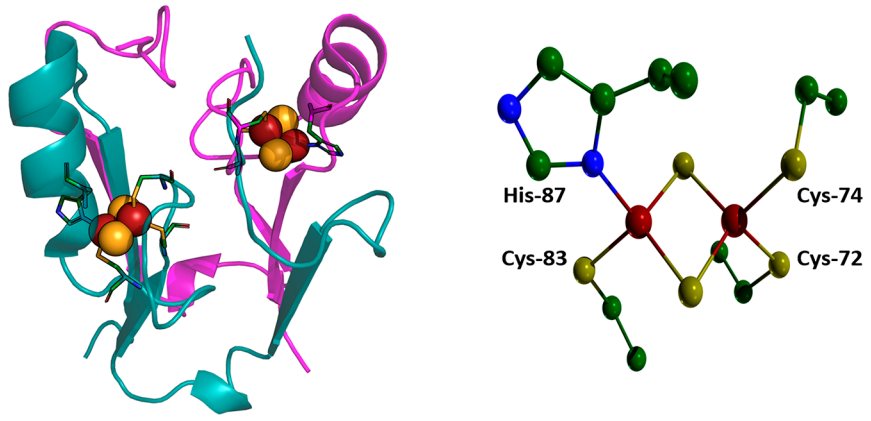

Figure 1. Cluster binding domain for mNT (left). Close-up of the 3Cys:1His [2Fe-2S] cluster up to the C_α atom of each residue with hydrogens omitted (right). The structures shown are based on Protein Data Bank entry2QH7.[13]

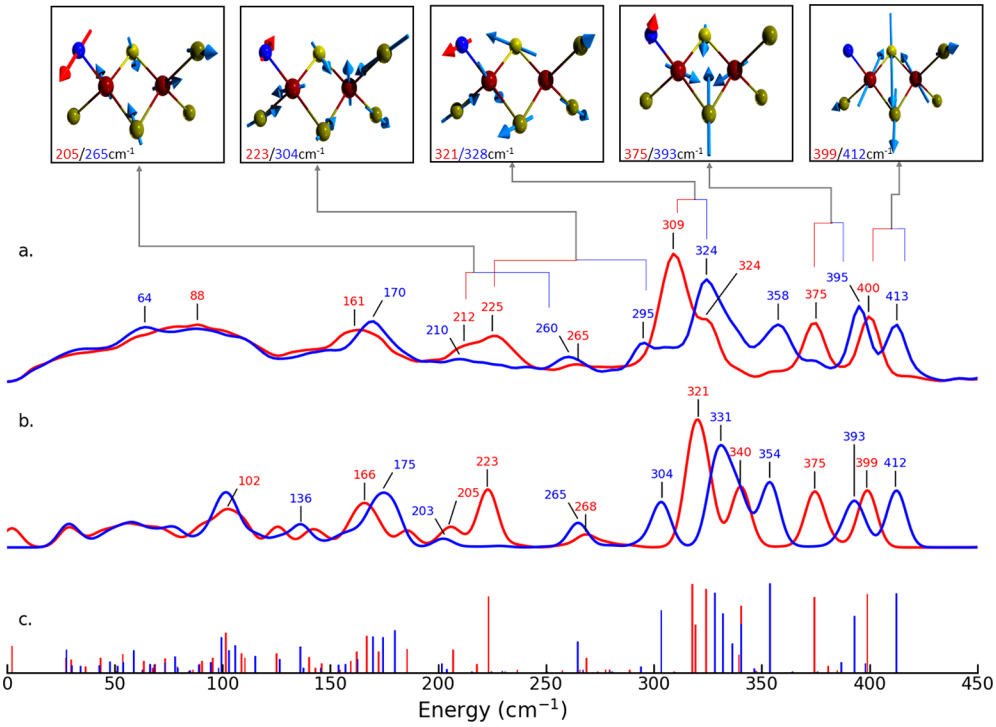

Figure 2. ^{57}Fe PVDOS for oxidized (blue) and reduced (red) mNT. (a) Experimental ^{57}Fe PVDOS (NRVS) spectrum. (b) DFT-calculated ^{57}Fe PVDOS spectrum. (c) Individual ^{57}Fe PVDOS-calculated transitions. The top inset shows the DFT-calculated vibrational motion (arrows) and frequencies for the [2Fe-2S] core with lines indicating their experimental assignment in the oxidized and reduced forms. The motion depicted is of the $[2Fe\text{-}2S]^{2+}$ oxidized state calculation. Labels in the DFT-derived spectrum reflect band positions for comparison to experiment; the individual mode energies are listed in Table S1.

reduced form of mNT at pH 6.7 using NRVS, because this pH represents a good balance between cluster stability and physiological relevance.[12] The NRVS data for oxidized and reduced mNT are presented in Figure 2a. As previously observed with [2Fe-2S] Fds, the low-frequency bands in the range of 50−120 cm^{-1} correspond to large scale protein motions and torsional modes of the [2Fe-2S] cluster, while the features from ∼120 to 180 cm^{-1} involve significant bending motion.[26] At the other extreme, modes around ∼400 cm^{-1} involve stretching of the Fe centers together with bridging sulfides (S_b). Upon reduction, the bands are generally red-shifted by 10−20 cm^{-1}, although there is not an exact 1:1 correspondence in modes consistent with other Fe−S clusters.[27] For the oxidized spectrum, there is fair correspondence with the previously reported Raman spectrum (Table S1).[23]

Qualitative assignment of the major features for the oxidized sample can be performed by comparison with previous NRVS and Raman results on [2Fe-2S] Fds (Table S1). A pair of high-frequency bands (413 and 395 cm^{-1}) align with similar bands in *Rc*6 Fd.[26] From the literature, these have been assigned to asymmetric and symmetric motions of the [2Fe-2S] core, respectively.[26,28] The middle-frequency bands (∼300−373 cm^{-1}) correspond mostly to various mixtures of Fe−S_t(Cys) and Fe−S_b stretching motions.[28] The 295 cm^{-1} feature is not seen in the *Rc*6 Fd spectrum, but bands at 284 and 293 cm^{-1} are seen in the Raman spectrum of mNT; they are presumably

https://doi.org/10.1021/acs.biochem.1c00252
Biochemistry 2021, 60, 2419−2424

Fe−S_t(Cys) stretches "influenced by the presence of the Fe-His moiety".[23]

The NRVS band at 260 cm^{-1} has no correspondence in conventional Fd spectra, but it can be related to bands seen at 267 and 265−274 cm^{-1} in mNT[23] and Rieske protein[29] Raman spectra, respectively. In the latter case, bands at 266 and 274 cm^{-1} were assigned to protonated hydrogen-bonded imidazole and deprotonated hydrogen-bonded imidazolate, respectively, both ligated to Fe with water serving as the H-bond donor and/or acceptor.[30]

The reduced mNT NRVS shows the expected shifts to lower frequencies that were seen in Fd proteins (Figure 2a).[26] The primary Fe−S_b bands shift by 13 and 20 cm^{-1} to 400 and 375 cm^{-1}, respectively, approximately the same as seen in Fds. Similar shifts are also seen in the Fe−S_t(Cys) region. The most dramatic shift is the presumed Fe−N_δ(His) band migration from 260 cm^{-1} to 225 and 212 cm^{-1}. Because it is the His-ligated Fe that is redox active,[21] the latter bands can be ascribed to the Fe(II)−N_δ(His) motion.

Observation of this candidate Fe(II)−N_δ(His) mode illustrates an advantage of the NRVS technique: the reduced species exhibits contributions to the NRVS signal of similar quality from the Fe(II) and Fe(III) sites. In contrast, although resonance Raman spectra of reduced Rieske proteins have been reported,[29,30] in both cases the authors concluded that the spectrum primarily reports on the Fe(III) site of this mixed valence species, because this is the source of the resonantly excited S → Fe charge transfer band. NRVS allows inspection of the mNT Fe(II)−N_{his} vibrational modes for the first time.

Analogies can be made to the resonance Raman spectra of deoxy-myoglobin (Mb), which also contains a high-spin Fe(II)−histidine bond. Bands at 210, 218, and 225 cm^{-1} have been reported for deoxy-Mb at 150 K (or 213, 220, and 226 cm^{-1})[31] and assigned to different conformational substates with respect to the Fe−His bond.[32] It is unclear if the pair of features at 212 and 225 cm^{-1} in the reduced mNT spectrum might analogously represent different conformations; for more detailed insights into these features, we turned to DFT calculations.

We performed DFT calculations on a truncated model of mNT, involving the [2Fe-2S] cluster and its immediate protein environment (Figure S1). The model includes the amino acid backbone linking the four residues directly coordinating the [2Fe-2S] core, with the noncoordinating residues truncated to their C_α atoms (equivalent to alanine residues). The $[2Fe\text{-}2S]^{2+}$ and $[2Fe\text{-}2S]^{+}$ states were calculated with and without protonation of the Fe-coordinating histidine (His-87). Regardless of the noncoordinating nitrogen N_ε(His-87) protonation status, our calculations indicated the histidine-bound iron to be the redox active metal site, which is reminiscent of reduced Rieske clusters in which the two-histidine-bound Fe is reduced (see the Supporting Information for details and alternative DFT models).[33] The best agreement with our experimental data is achieved by models with a coordinating histidine imidazole for the reduced form and an imidazolate for the oxidized forms, as shown by the simulated NRVS profiles in Figure 2b. The protonation of the histidine upon reduction at the pH 6.7 level is consistent with previous pulsed EPR studies.[21]

For the oxidized cluster, starting from a high energy, the 413 and 395 cm^{-1} bands are confirmed to be asymmetric and symmetric Fe−S modes of the entire $[2Fe\text{-}2S]^{2+}$ core, respectively (Supporting Information, animated vibrational modes). The experimental pair of bands at 358 and 324 cm^{-1} are dominantly Fe−S_t/N_δ(His) asymmetric stretching modes with the former mode strongly coupled to Fe−S_b motion and the latter representing the most intense feature in the spectrum. The intensity at 295 cm^{-1} is of special note; inspection of the corresponding DFT mode reveals a substantial Fe(III)−N_δ(His) stretching character weakly coupled to Fe−S_b scissoring motion and Fe−S_t stretching motion. Likewise, another experimental feature at 260 cm^{-1} similarly features Fe−N_δ(His) stretching, but with much less coupling to Fe−S_t motion than the feature at 295 cm^{-1} resulting in a lower ^{57}Fe PVDOS. A distribution of the Fe−N_δ stretching-related modes in this region is consistent with previous resonance Raman data.[23]

The experimental intensity observed at 170 cm^{-1} in the oxidized cluster is predicted to be composed of multiple vibrational modes. These modes are essentially Fe−S_t/N_δ bending modes with the Fe atoms wagging relative to the coordinating amino acids. Below 100 cm^{-1}, a broad intensity is observed that is composed of strongly delocalized vibrations coupled to the protein backbone. Such modes are not predicted by the truncated models used by DFT; however, we do note that our simulations predict another bending mode (calculated at 102 cm^{-1}) with the Fe and coordinating amino acids moving in a twisting motion that contributes significant intensity in this region.

Upon reduction and protonation of the coordinating imidazole, our calculations verify a shift of the high-energy (>300 cm^{-1}) Fe−S cluster modes to a lower energy, with their characters otherwise similar to those of the oxidized state modes. The NRVS band at 295 cm^{-1} in the oxidized cluster is not present in the reduced system, implying a change in the Fe−N_δ bonding. There are two modes in the reduced spectrum calculated at 223 cm^{-1} (Figure 3) and 205 cm^{-1},

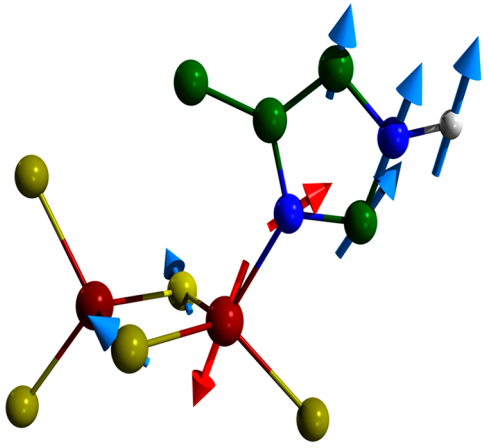

Figure 3. Reduced $[2Fe\text{-}2S]^{+}$ state mNT mode calculated at 223 cm^{-1}, showing the Fe(II)−N_δ(His) stretch. Only the [2Fe-2S] and His-87 fragments of the DFT model are shown.

which upon inspection correspond to the modes at 304 and 265 cm^{-1}, respectively, calculated for the oxidized cluster. Although the core [2Fe-2S] motion is similar, the reduction increases amount of motion of both the directly cluster-coordinating and intervening amino acids (Figure S1). Finally, the low-energy region for the reduced cluster is again composed of various Fe−N_δ, Fe−S_t, and Fe−S_b bending

https://doi.org/10.1021/acs.biochem.1c00252
Biochemistry 2021, 60, 2419−2424

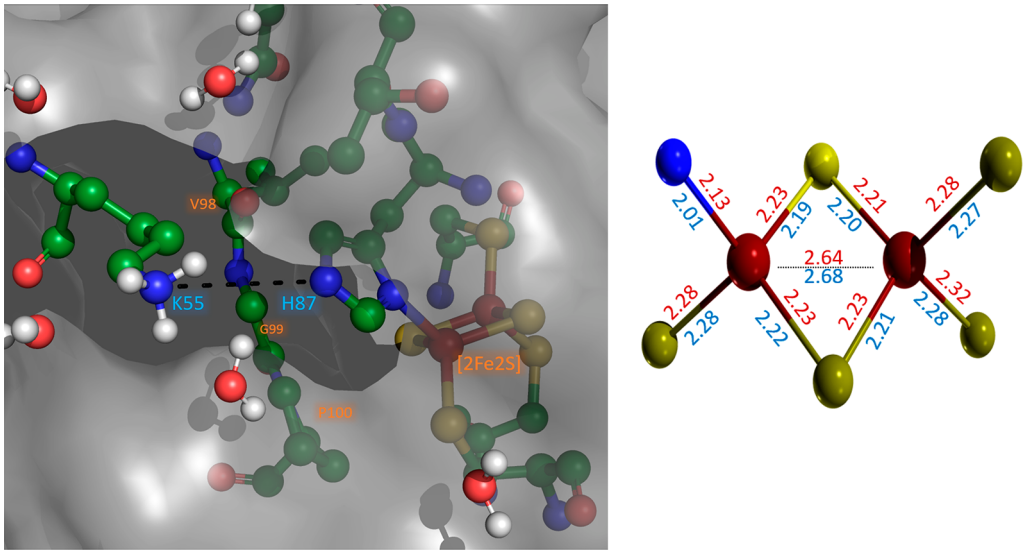

Figure 4. His-87 and Lys-55 (left) with the protein cleft (Val-98, Gly-99, and Pro-100), where gray represents the Connolly[36] (solvent access) surface excluding His-87 and Lys-55 and the dashed black line connects the two heavy (nitrogen) atoms within hydrogen bonding distance as found in Protein Data Bank entry 2QH7.[13] Geometry-optimized structure of the mNT [2Fe-2S] cluster (right). Labels indicate bond lengths (Å) for the oxidized imidazolate-bound (blue) and reduced imidazole-bound (red) clusters.

modes with the strongest contribution from the Fe−S_t/N_δ wagging motion.

The decrease in the frequency of the Fe−N_δ-derived vibrations is consistent with our geometry-optimized structure for the reduced cluster that predicts a 0.12 Å increase in the Fe−N_δ(His) bond length upon cluster reduction and concomitant protonation of His-87 (Supporting Information, DFT structures). This is consistent with the greater donor character of imidazolate than of imidazole.

DISCUSSION

Previous work on holo-mNT in the oxidized and reduced states revealed very little modification of the tertiary and quaternary structures between the two forms.[19] This fact is consistent with the minimal redox-dependent changes in the low-energy region of the NRVS spectra that reflect diffuse vibrations strongly coupled to the protein backbone. The holo-mNT has been shown to be susceptible to cluster loss under oxidizing conditions,[5] and it has been proposed previously that Fe−N_δ(His) bond scission at low pH could operate as a first step of cluster loss.[23] Our results verify that the Fe−His bond is stronger in the oxidized state than in the reduced state, and at first glance, the increased lability of the oxidized [2Fe-2S] mNT cluster (relative to that of its reduced form) seems paradoxical.

Previously, it has been observed in deoxyMb that iron−histidine bond cleavage is driven by solvation and unfolding of the active site at lower pH rather than protonation of the Fe-coordinating imidazole.[34] One possible opportunity for the loss of the mNT cluster is the compression of the cluster upon oxidation. The nearby Lys-55 (from the other monomer), near the [2Fe-2S]-coordinating His-87, has been purported to dynamically hydrogen bond to the imidazolate and protect it from solvent exposure.[25] Our geometry-optimized structures, which reflect our experimental NRVS data, demonstrate a shortening of the Fe−N_δ bond and of the opposing Fe−S_t bonds on the opposite side of the cluster (Figure 4, right).

We found that including protonation of the N_ε atom to imidazole in the oxidized form in our DFT calculation leads to a relative increase of 0.06 Å in the length of the Fe−N_δ bond that is still 0.06 Å shorter than that of the reduced cluster. This lengthening reflects an increased labilization of the bond and possibly contributes to the pH dependence of the cluster loss. Likewise, protonation to imidazole would eliminate the direct N_ε···Lys-55 H-bonding.[25]

Collectively, this implies that when the reduced cluster is oxidized under non-acidic conditions to $[2Fe\text{-}2S]^{2+}$ there is a compression of the cluster geometry and coordinating histidine. Although not dramatically different, this new geometry decreases the dynamic residence time of the hydrogen bond between His-87 and Lys-55 (Figure 4, left), allowing greater access of the solvent to the protein cleft between the two amino acids (relative to the reduced form). Greater solvent access provides enthalpic pressure for Fe−N_δ bond rupture.[25] Additionally, at lower pH values, the cluster-bound imidazole cannot interact with Lys-55 and the cleft can be dynamically solvated more frequently;[25] this is concomitant with the increased level of destabilization of the Fe−N_δ bond due to the reduced donor character of imidazole versus imidazolate to the Fe atom that would lead to enhanced geminate release of the $[2Fe\text{-}2S]^{2+}$ cluster. This mechanism explains the redox-dependent cluster loss and how it is enabled by a lower pH in mNT but will require additional structural studies for confirmation. However, the model is consistent with many existing mutagenesis studies of the critical Lys-55. Substitution with a guanidinium, K55R,[24] showed a cluster stability similar to that of the wild type expected of a similar H-bonding pattern; conversion to the aliphatic residue, K55I,[35] led to cluster stability that was greater than that of the wild type, which is consistent with the decreased polarity of the protein cleft gated by K55 and H87 (Figure 4, left), and conversion to an anionic residue, K55E,[11] revealed cluster transfer that was slower than that of the wild type.

SUMMARY

Here we have demonstrated the utility of ^{57}Fe NRVS in probing the Fe−His interaction in both the reduced and the oxidized mNT [2Fe-2S] cluster. Unlike resonance Raman

https://doi.org/10.1021/acs.biochem.1c00252
Biochemistry 2021, 60, 2419−2424

spectroscopy, NRVS does not depend on optical excitations, and thus, we were able to characterize the reduced Fe−N_δ bond for the first time; it does not have excitation bands amenable to resonance Raman,[23] and there are no crystal structures available for the mNT in the reduced state. The Fe−N bond is stronger in the oxidized form; however, the protein is more susceptible to cluster loss in this form.[19] We identify the dynamic solvation of the protein cleft proximal to the cluster-coordinating histidine as a potential factor facilitating cluster loss consistent with previous molecular dynamics studies.[25] This work highlights the strengths of ^{57}Fe NRVS to obtain detailed geometric and vibrational insights into Fe−S clusters that cannot be accessed through conventional methods.

■ ASSOCIATED CONTENT

Supporting Information

The Supporting Information is available free of charge at https://pubs.acs.org/doi/10.1021/acs.biochem.1c00252.

Experimental and computational procedures, Figures S1−S4, and Table S1 (PDF)

Cartesian (XYZ format) coordinates of the DFT-optimized structures (ZIP)

Animations (GIF format) showing the DFT-calculated normal modes (ZIP)

Accession Codes

MitoNEET−CISD1, UniProt entry Q9NZ45.

■ AUTHOR INFORMATION

Corresponding Author

Stephen P. Cramer − *SETI Institute, Mountain View, California 94043, United States;* orcid.org/0000-0002-3751-7623; Email: scramer@seti.org

Authors

Leland B. Gee − *LCLS, SLAC National Accelerator Laboratory, Menlo Park, California 94025, United States;* orcid.org/0000-0002-5817-3997

Vladimir Pelmenschikov − *Institut für Chemie, Technische Universität Berlin, 10623 Berlin, Germany;* orcid.org/0000-0002-0523-4418

Cécile Mons − *Institut de Chimie des Substances Naturelles (ICSN), CNRS UPR 2301, Université Paris-Saclay, 91198 Gif-sur-Yvette, France*

Nakul Mishra − *Department of Chemistry, University of California, Davis, California 95616, United States*

Hongxin Wang − *SETI Institute, Mountain View, California 94043, United States*

Yoshitaka Yoda − *Precision Spectroscopy Division, SPring-8/JASRI, Sayo, Hyogo 679-5198, Japan*

Kenji Tamasaku − *Precision Spectroscopy Division, SPring-8/JASRI, Sayo, Hyogo 679-5198, Japan; RIKEN SPring-8 Center, Sayo-gun, Hyogo 679-5148, Japan*

Marie-Pierre Golinelli-Cohen − *Institut de Chimie des Substances Naturelles (ICSN), CNRS UPR 2301, Université Paris-Saclay, 91198 Gif-sur-Yvette, France;* orcid.org/0000-0002-6738-8631

Complete contact information is available at: https://pubs.acs.org/10.1021/acs.biochem.1c00252

Funding

The work by V.P. was funded by the Deutsche Forschungsgemeinschaft (DFG, German Research Foundation) under Germany's Excellence Strategy (EXC 2008-390540038, UniSysCat). M.-P.G.-C. warmly acknowledges the networking support from the EU COST Action FeSBioNet (CA15133). S.P.C. was funded by National Institutes of Health Grant GM65440.

Notes

The authors declare no competing financial interest.

■ ACKNOWLEDGMENTS

Some computational work was performed under the XSIM project on the CORI computing system at NERSC, a U.S. Department of Energy Office of Science User Facility operated under Contract DE-AC02-05CH11231.

■ REFERENCES

(1) Tamir, S., Paddock, M. L., Darash-Yahana-Baram, M., Holt, S. H., Sohn, Y. S., Agranat, L., Michaeli, D., Stofleth, J. T., Lipper, C. H., Morcos, F., Cabantchik, I. Z., Onuchic, J. N., Jennings, P. A., Mittler, R., and Nechushtai, R. (2015) Structure-function analysis of NEET proteins uncovers their role as key regulators of iron and ROS homeostasis in health and disease. *Biochim. Biophys. Acta, Mol. Cell Res. 1853* (6), 1294−1315.

(2) Colca, J. R., McDonald, W. G., Waldon, D. J., Leone, J. W., Lull, J. M., Bannow, C. A., Lund, E. T., and Mathews, W. R. (2004) Identification of a novel mitochondrial protein ("mitoNEET") cross-linked specifically by a thiazolidinedione photoprobe. *Am. J. Physiol. Endocrinol. Metab. 286* (2), E252−E260.

(3) Moreno-Navarrete, J. M., Moreno, M., Ortega, F., Sabater, M., Xifra, G., Ricart, W., and Fernandez-Real, J. M. (2016) CISD1 in association with obesity-associated dysfunctional adipogenesis in human visceral adipose tissue. *Obesity 24* (1), 139−147.

(4) Kusminski, C. M., Holland, W. L., Sun, K., Park, J., Spurgin, S. B., Lin, Y., Askew, G. R., Simcox, J. A., McClain, D. A., Li, C., and Scherer, P. E. (2012) MitoNEET-driven alterations in adipocyte mitochondrial activity reveal a crucial adaptive process that preserves insulin sensitivity in obesity. *Nat. Med. 18* (10), 1539−U144.

(5) Ferecatu, I., Gonçalves, S., Golinelli-Cohen, M.-P., Clémancey, M., Martelli, A., Riquier, S., Guittet, E., Latour, J.-M., Puccio, H., Drapier, J.-C., Lescop, E., and Bouton, C. (2014) The Diabetes Drug Target MitoNEET Governs a Novel Trafficking Pathway to Rebuild an Fe-S Cluster into Cytosolic Aconitase/Iron Regulatory Protein 1. *J. Biol. Chem. 289* (41), 28070−28086.

(6) Chen, X. Y., Ren, H. H., Wang, D., Chen, Y., Qu, C. J., Pan, Z. H., Liu, X. N., Hao, W. J., Xu, W. J., Wang, K. J., Li, D. F., and Zheng, Q. S. (2019) Isoliquiritigenin Induces Mitochondrial Dysfunction and Apoptosis by Inhibiting mitoNEET in a Reactive Oxygen Species-Dependent Manner in A375 Human Melanoma Cells. *Oxid. Med. Cell. Longevity 2019*, 9817576.

(7) Sohn, Y. S., Tamir, S., Song, L. H., Michaeli, D., Matouk, I., Conlan, A. R., Harir, Y., Holt, S. H., Shulaev, V., Paddock, M. L., Hochberg, A., Cabanchick, I. Z., Onuchic, J. N., Jennings, P. A., Nechushtai, R., and Mittler, R. (2013) NAF-1 and mitoNEET are central to human breast cancer proliferation by maintaining mitochondrial homeostasis and promoting tumor growth. *Proc. Natl. Acad. Sci. U. S. A. 110* (36), 14676−14681.

(8) Karmi, O., Marjault, H. B., Pesce, L., Carloni, P., Onuchic, J. N., Jennings, P. A., Mittler, R., and Nechushtai, R. (2018) The unique fold and lability of the 2Fe-2S clusters of NEET proteins mediate their key functions in health and disease. *JBIC, J. Biol. Inorg. Chem. 23* (4), 599−612.

(9) Mittler, R., Darash-Yahana, M., Sohn, Y. S., Bai, F., Song, L. H., Cabantchik, I. Z., Jennings, P. A., Onuchic, J. N., and Nechushtai, R. (2019) NEET Proteins: A New Link Between Iron Metabolism,

Reactive Oxygen Species, and Cancer. *Antioxid. Redox Signaling 30* (8), 1083−1095.
(10) Geldenhuys, W. J., Benkovic, S. A., Lin, L., Yonutas, H. M., Crish, S. D., Sullivan, P. G., Darvesh, A. S., Brown, C. M., and Richardson, J. R. (2017) MitoNEET (CISD1) Knockout Mice Show Signs of Striatal Mitochondrial Dysfunction and a Parkinson's Disease Phenotype. *ACS Chem. Neurosci. 8* (12), 2759−2765.
(11) Zuris, J. A., Harir, Y., Conlan, A. R., Shvartsman, M., Michaeli, D., Tamir, S., Paddock, M. L., Onuchic, J. N., Mittler, R., Cabantchik, Z. I., Jennings, P. A., and Nechushtai, R. (2011) Facile transfer of 2Fe-2S clusters from the diabetes drug target mitoNEET to an apo-acceptor protein. *Proc. Natl. Acad. Sci. U. S. A. 108* (32), 13047−13052.
(12) Mons, C., Botzanowski, T., Nikolaev, A., Hellwig, P., Cianferani, S., Lescop, E., Bouton, C., and Golinelli-Cohen, M. P. (2018) The H_2O_2-Resistant Fe-S Redox Switch MitoNEET Acts as a pH Sensor to Repair Stress-Damaged Fe-S Protein. *Biochemistry 57* (38), 5616−5628.
(13) Paddock, M. L., Wiley, S. E., Axelrod, H. L., Cohen, A. E., Roy, M., Abresch, E. C., Capraro, D., Murphy, A. N., Nechushtai, R., Dixon, J. E., and Jennings, P. A. (2007) MitoNEET is a uniquely folded 2Fe-2S outer mitochondrial membrane protein stabilized by pioglitazone. *Proc. Natl. Acad. Sci. U. S. A. 104* (36), 14342−14347.
(14) Hou, X. W., Liu, R. J., Ross, S., Smart, E. J., Zhu, H. N., and Gong, W. M. (2007) Crystallographic studies of human MitoNEET. *J. Biol. Chem. 282* (46), 33242−33246.
(15) Lin, J. Z., Zhou, T., Ye, K. Q., and Wang, J. F. (2007) Crystal structure of human mitoNEET reveals distinct groups of iron-sulfur proteins. *Proc. Natl. Acad. Sci. U. S. A. 104* (37), 14640−14645.
(16) Bak, D. W., Zuris, J. A., Paddock, M. L., Jennings, P. A., and Elliott, S. J. (2009) Redox characterization of the FeS protein MitoNEET and impact of thiazolidinedione drug binding. *Biochemistry 48* (43), 10193−10195.
(17) Bak, D. W., and Elliott, S. J. (2014) Alternative FeS cluster ligands: tuning redox potentials and chemistry. *Curr. Opin. Chem. Biol. 19*, 50−58.
(18) Bergner, M., Dechert, S., Demeshko, S., Kupper, C., Mayer, J. M., and Meyer, F. (2017) Model of the MitoNEET [2Fe-2S] Cluster Shows Proton Coupled Electron Transfer. *J. Am. Chem. Soc. 139* (2), 701−707.
(19) Golinelli-Cohen, M. P., Lescop, E., Mons, C., Goncalves, S., Clemancey, M., Santolini, J., Guittet, E., Blondin, G., Latour, J. M., and Bouton, C. (2016) Redox Control of the Human Iron-Sulfur Repair Protein MitoNEET Activity via Its Iron-Sulfur Cluster. *J. Biol. Chem. 291* (14), 7583−7593.
(20) Wiley, S. E., Paddock, M. L., Abresch, E. C., Gross, L., van der Geer, P., Nechushtai, R., Murphy, A. N., Jennings, P. A., and Dixon, J. E. (2007) The outer mitochondrial membrane protein mitoNEET contains a novel redox-active 2Fe-2S cluster. *J. Biol. Chem. 282* (33), 23745−23749.
(21) Dicus, M. M., Conlan, A., Nechushtai, R., Jennings, P. A., Paddock, M. L., Britt, R. D., and Stoll, S. (2010) Binding of histidine in the (Cys)3(His)1-coordinated [2Fe-2S] cluster of human mitoNEET. *J. Am. Chem. Soc. 132* (6), 2037−2049.
(22) Iwasaki, T., Samoilova, R. I., Kounosu, A., Ohmori, D., and Dikanov, S. A. (2009) Continuous-wave and pulsed EPR characterization of the [2Fe-2S](Cys)3(His)1 cluster in rat MitoNEET. *J. Am. Chem. Soc. 131* (38), 13659−13667.
(23) Tirrell, T. F., Paddock, M. L., Conlan, A. R., Smoll, E. J., Nechushtai, R., Jennings, P. A., and Kim, J. E. (2009) Resonance Raman Studies of the (His)(Cys)(3) 2Fe-2S Cluster of MitoNEET: Comparison to the (Cys)(4) Mutant and Implications of the Effects of pH on the Labile Metal Center. *Biochemistry 48* (22), 4747−4752.
(24) Baxter, E. L., Zuris, J. A., Wang, C., Vo, P. L. T., Axelrod, H. L., Cohen, A. E., Paddock, M. L., Nechushtai, R., Onuchic, J. N., and Jennings, P. A. (2013) Allosteric control in a metalloprotein dramatically alters function. *Proc. Natl. Acad. Sci. U. S. A. 110* (3), 948−953.
(25) Pesce, L., Calandrini, V., Marjault, H. B., Lipper, C. H., Rossetti, G., Mittler, R., Jennings, P. A., Bauer, A., Nechushtai, R., and Carloni, P. (2017) Molecular Dynamics Simulations of the 2Fe-2S Cluster-Binding Domain of NEET Proteins Reveal Key Molecular Determinants That Induce Their Cluster Transfer/Release. *J. Phys. Chem. B 121* (47), 10648−10656.
(26) Xiao, Y., Tan, M.-L., Ichiye, T., Wang, H., Guo, Y., Smith, M. C., Meyer, J., Sturhahn, W., Alp, E. E., Zhao, J., Yoda, Y., and Cramer, S. P. (2008) Dynamics of *Rhodobacter capsulatus* [2Fe-2S] Ferredoxin VI and *Aquifex aeolicus* Ferredoxin 5 *via* Nuclear Resonance Vibrational Spectroscopy (NRVS) and Resonance Raman Spectroscopy. *Biochemistry 47* (25), 6612−6627.
(27) Lauterbach, L., Gee, L. B., Pelmenschikov, V., Jenney, F. E., Kamali, S., Yoda, Y., Adams, M. W., and Cramer, S. P. (2016) Characterization of the [3Fe-4S](0/1+) cluster from the D14C variant of Pyrococcus furiosus ferredoxin via combined NRVS and DFT analyses. *Dalton Trans. 45* (17), 7215−7219.
(28) Han, S., Czernuszewicz, R. S., Kimura, T., Adams, M. W. W., and Spiro, T. G. (1989) Fe_2S_2 Protein Resonance Raman Revisited: Structural Variations among Adrenodoxin, Ferredoxin, and Red Paramagnetic Protein. *J. Am. Chem. Soc. 111* (10), 3505−3511.
(29) Rotsaert, F. A. J., Pikus, J. D., Fox, B. G., Markley, J. L., and Sanders-Loehr, J. (2003) N-isotope effects on the Raman spectra of Fe_2S_2 ferredoxin and Rieske ferredoxin: evidence for structural rigidity of metal sites. *JBIC, J. Biol. Inorg. Chem. 8* (3), 318−326.
(30) Kuila, D., Schoonover, J. R., Dyer, R. B., Batie, C. J., Ballou, D. P., Fee, J. A., and Woodruff, W. H. (1992) Resonance Raman Studies of Rieske-Type Proteins. *Biochim. Biophys. Acta, Bioenerg. 1140* (2), 175−183.
(31) Schott, J., Dreybrodt, W., and Schweitzer-Stenner, R. (2001) The Fe2+-HiS(F8) Raman band shape of deoxymyoglobin reveals taxonomic conformational substates of the proximal linkage. *Biophys. J. 81* (3), 1624−1631.
(32) Gilch, H., Schweitzerstenner, R., and Dreybrodt, W. (1993) Structural Heterogeneity of the Fe2+-N-Epsilon(His(F8)) Bond in Various Hemoglobin And Myoglobin Derivatives Probed by the Raman-Active Iron Histidine Stretching Mode. *Biophys. J. 65* (4), 1470−1485.
(33) Gurbiel, R. J., Batie, C. J., Sivaraja, M., True, A. E., Fee, J. A., Hoffman, B. M., and Ballou, D. P. (1989) Electron-nuclear double resonance spectroscopy of nitrogen-15-enriched phthalate dioxygenase from Pseudomonas cepacia proves that two histidines are coordinated to the [2Fe-2S] Rieske-type clusters. *Biochemistry 28* (11), 4861−4871.
(34) Tang, Q., Kalsbeck, W. A., Olson, J. S., and Bocian, D. F. (1998) Disruption of the Heme Iron−Proximal Histidine Bond Requires Unfolding of Deoxymyoglobin. *Biochemistry 37* (19), 7047−7056.
(35) Bak, D. W., and Elliott, S. J. (2013) Conserved Hydrogen Bonding Networks of MitoNEET Tune Fe-S Cluster Binding and Structural Stability. *Biochemistry 52* (27), 4687−4696.
(36) Connolly, M. L. (1983) Analytical molecular surface calculation. *J. Appl. Crystallogr. 16* (5), 548−558.

https://doi.org/10.1021/acs.biochem.1c00252
Biochemistry 2021, 60, 2419−2424